Journal of Nuclear Medicine, published on December 20, 2019 as doi:10.2967/jnumed.119.234708

Early Detection in a Mouse Model of Pancreatic Cancer by Imaging DNA Damage Response Signalling

James C. Knight[1,2], Julia Baguña Torres[1], Robert Goldin[3], Michael Mosley[1], Gemma M. Dias[1], Luisa Contreras Bravo[1], Veerle Kersemans[1], P. Danny Allen[1], Somnath Mukherjee[1], Sean Smart[1], and Bart Cornelissen[1†]

[1] CR-UK/MRC Oxford Institute for Radiation Oncology, Department of Oncology, University of Oxford, Oxford, United Kingdom

[2] School of Natural and Environmental Sciences, Newcastle University, Newcastle upon Tyne, United Kingdom

[3] Department of Histopathology, Imperial College London, St Mary's Hospital Campus, London, United Kingdom

[†] **To whom correspondence should be addressed:**
Dr. Bart Cornelissen
CRUK/MRC Oxford Institute for Radiation Oncology
Department of Oncology
University of Oxford
Old Road Campus Research Building
Off Roosevelt Drive
Oxford OX3 7LJ
Tel: +44 (0)1865 857126
Fax: +44 (0)1865 857127
Email: bart.cornelissen@oncology.ox.ac.uk
ORCID ID: 0000-0001-7581-3303

1st author, not in training

Dr. James Knight
CRUK/MRC Oxford Institute for Radiation Oncology
Department of Oncology
University of Oxford
Old Road Campus Research Building
Off Roosevelt Drive
Oxford OX3 7LJ
Tel: +44 (0)1865 857126
Fax: +44 (0)1865 857127
Email: james.knight@oncology.ox.ac.uk

Word count: 4,561
Running title: Early Detection of PDAC in KPC Mice
Key words: Pancreatic Ductal Adenocarcinoma, PET, SPECT, DNA Damage Repair, γH2AX
Financial Support: This research was supported by CRUK through the Oxford Institute for Radiation Oncology and the CRUK Oxford Centre, and the CRUK/EPSRC Imaging Centre in Oxford. Further support was obtained from Pancreatic Cancer UK (BC, LCB) and Pancreatic Cancer Research Fund (BC, JBT).

The authors disclose no potential conflicts of interest

ABSTRACT

Rationale: Despite its widespread use in oncology, the PET radiotracer ^{18}F-FDG is ineffective for improving early detection of pancreatic ductal adenocarcinoma (PDAC). An alternative strategy for early detection of pancreatic cancer involves visualisation of high-grade pancreatic intraepithelial neoplasias (PanIN-3), generally regarded as the non-invasive precursors of PDAC. The DNA damage response is known to be hyper-activated in late-stage PanINs. Therefore, we investigated whether the SPECT imaging agent, ^{111}In-anti-γH2AX-TAT, allows visualisation of the DNA damage repair marker γH2AX in PanIN-3s in an engineered mouse model of PDAC, to facilitate early detection of PDAC.

Methods: Genetically engineered KPC mice ($KRas^{LSL.G12D/+}$; $p53^{LSL.R172H/+}$; PdxCre) were imaged with ^{18}F-FDG and ^{111}In-anti-γH2AX-TAT. PanIN/PDAC presence visualised by histology was compared with autoradiography and immunofluorescence. Separately, the survival of KPC mice imaged with ^{111}In-anti-γH2AX-TAT was evaluated.

Results: In KPC mouse pancreata, γH2AX expression was increased in high-grade PanINs, but not in PDAC, corroborating earlier results obtained from human pancreas sections. Uptake of ^{111}In-anti-γH2AX-TAT, but not ^{111}In-IgG-TAT or ^{18}F-FDG, within the pancreas was positively correlated with the age of KPC mice, which was correlated with the number of high-grade PanINs. ^{111}In-anti-γH2AX-TAT localises preferentially in high-grade PanIN lesions, but not in established PDAC. Younger, non-tumour-bearing KPC mice that show uptake of ^{111}In-anti-γH2AX-TAT in the pancreas survive significantly shorter than mice with physiological ^{111}In-anti-γH2AX-TAT uptake.

Conclusion: ^{111}In-anti-γH2AX-TAT imaging allows non-invasive detection of DNA damage repair signalling upregulation in pre-invasive PanIN lesions and is a promising new tool to aid in the early detection and staging of pancreatic cancer.

INTRODUCTION

Globally, the number of pancreatic cancer cases is predicted to reach 484,486 by 2020 (*1*). Approximately 90% of these patients will have pancreatic ductal adenocarcinoma (PDAC) which has a dismal 5-year survival rate of <5% (*2*). PDAC is projected to become the second-most frequent cause of cancer-related death by 2030. As current PDAC therapies are only minimally effective, the best chance of a cure is surgical resection. Most patients, however, are ineligible for surgery as they are diagnosed at an advanced stage, when the cancer has already spread beyond the pancreas. Encouragingly, if PDAC is detected when it is still confined to the pancreas, in approximately 15% of cases, the 5-year survival rate following surgery markedly increases to 25% (*3*), and may be improved even further by neoadjuvant chemotherapy (*4*). Therefore, the most effective strategy for improving PDAC survival is to detect its presence earlier so that more patients can benefit from life-extending and potentially curative surgery.

Pancreatic cancer diagnosis usually depends on anatomical imaging techniques such as computed tomography, endoscopic retrograde cholangiopancreatography, endoscopic ultrasound, laparoscopy, and magnetic resonance imaging (*5*). This information is then used in conjunction with analysis of serum biomarkers (such as CA19-9 (*6*)) and biopsied tissue to confirm the diagnosis and stage of the disease (*5*). A major limitation of the aforementioned imaging techniques is that none are sufficiently sensitive to reliably detect the molecular biomarkers of PDAC formation which arise before the manifestation of anatomical abnormalities (*7*). In contrast, nuclear imaging techniques such as positron emission tomography (PET) and single photon computed tomography (SPECT) do offer the required sensitivity (*7*). Unfortunately, however, the most widely utilised PET imaging agent, ^{18}F-fludeoxyglucose (^{18}F-FDG), has been found to be ineffective for improving early detection of PDAC (*7,8*). The failure of this agent – which reveals

abnormal glucose metabolism – is largely due to its inability to distinguish PDAC from chronic inflammation associated with focal mass-forming pancreatitis (*8*).

An emerging alternative strategy for early detection of PDAC involves detection of high-grade pancreatic intraepithelial neoplasias (PanIN-3) (*9*). Indeed, it has been suggested that the greatest hope for saving lives that otherwise would be lost to pancreatic cancer might be the early detection of PanIN precursor lesions (*10*). PanINs are the most common precursor of PDAC and range from PanIN-1-3 according to the degree of dysplasia (*10*).

High-grade PanIN-3 lesions have most diagnostic value as, unlike the lower grade lesions, these are more likely to culminate in invasive carcinoma, and are generally regarded as a canonical precursor to PDAC. Unlike PanIN-1 or -2, PanIN-3 lesions are present at very low frequencies in individuals with an otherwise healthy pancreas (4%), and then only in older patients, but more so in individuals with a familial background of PDAC (*11*), or with pancreatitis – known risk factors for PDAC (*12*), whereas PanIN-3s are present in 70% of PDAC patients. Given the difficulty to assess PanIN-3 burden non-invasively, no direct correlation with progression to PDAC can be made. However, a recent report using lineage analysis by Makohon-Moore et al. showed strong genetic relationships among high-grade PanINs, and PDAC lesions from the same patient (*13*), confirming the model of step-wise progression from PanIN-3 to PDAC (*14*). Taken together, this suggests that detection of PanIN-3 lesions may assist in early detection of PDAC tumorigenesis.

One attractive molecular biomarker of high-grade PanIN-3 lesions is the DNA damage response (DDR) protein γH2AX which arises through phosphorylation of the histone H2A variant H2AX, and is upregulated following cellular activation of DDR signalling . The DDR machinery, including γH2AX, is well-known to be elevated during the development of several cancer types

(*15,16*), including pancreatic cancer (*17*). Koorstra et al. showed that γH2AX has a favourable timeline of expression as an early detection biomarker as it is highly upregulated during the development of the pre-invasive PanIN-3 lesions and expressed far less in normal tissue and overt PDAC (*18*). Similar results were previously obtained by Bartkova et al., showing DDR activation in bladder, breast, and colon cancer precursor lesions (*15*).

We previously developed a SPECT imaging agent, ^{111}In-anti-γH2AX-TAT (*19-22*), and an alternative PET imaging agent, ^{89}Zr-anti-γH2AX-TAT (*23*), which permitted non-invasive visualisation and quantification of upregulated γH2AX during tumorigenesis in a mouse model of breast cancer (*20*), and monitoring of response to cancer therapy in mice bearing murine PDAC allograft tumours (*19*). Here, employment of the ^{111}In-labelled SPECT imaging agent allowed concommittant comparison by PET imaging with ^{18}F-FDG. In the present study, we demonstrate the potential of this DNA damage imaging agent for the detection of high-grade PanINs during PDAC development in the genetically engineered KPC ($KRas^{LSL.G12D/+}$; $p53^{LSL.R172H/+}$; PdxCre) mouse model, as a proxy for the human disease.

MATERIALS AND METHODS

Immunoconjugate preparation and radiosynthesis of ^{111}In-anti-γH2AX-TAT and ^{111}In-IgG-TAT was performed using previously described methods (*19*), from mouse monoclonal anti-γH2AX antibody (Merck, clone JBW-301), or isotype-matched IgG control antibody.

All animal procedures were performed in accordance with the UK Animals (Scientific Procedures) Act 1986 and with local ethical committee approval. Genetically engineered KPC mice (K-ras$^{LSL.G12D/+}$; p53$^{R172H/+}$; PdxCre) and BALB/c mice were housed in IVC cages in sex-matched groups of up to 5 per cage in an artificial day-night cycle facility with *ad libitum* access to food and water.

γH2AX imaging was performed 24 h after intravenous administration of ^{111}In-anti-γH2AX-TAT (5 MBq, 5 μg). ^{111}In-IgG-TAT (5 MBq, 5 μg) was used as a control. In some cases, mice were also concurrently imaged using ^{18}F-FDG (approximately 7.5 MBq), 1 h after intravenous administration. Mice were fasted 4 hours prior to ^{18}F-FDG injection. Groups of KPC mice were randomised for gender, whereas wild type mice (BALB/c) that were used as controls were all female. PET/SPECT/CT images were acquired using a VECTor^{4}CT scanner (MILabs, Utrecht, the Netherlands). For full experimental details, reconstruction and acquisition parameters, see Supporting Information.

At various ages (ranging from 70 to 224 days), KPC mice underwent concomitant imaging with ^{18}F-FDG, and ^{111}In-anti-γH2AX-TAT (n = 9) or ^{111}In-anti-IgG-TAT (n = 8). After imaging, pancreas tissue was harvested and processed as below.

To investigate the effect of pancreatic inflammation on ^{111}In-anti-γH2AX-TAT uptake, in a separate study, BALB/c mice (n = 4 per group) were administered caerulein *via* a series of six

hourly intraperitoneal injections to induce acute pancreatitis (*24*). ^{111}In-anti-γH2AX-TAT was administered intravenously 150 min after the last caerulein injection, and SPECT/CT imaging was performed 24 h later.

In addition, we performed a study comparing the biodistribution of ^{111}In-anti-γH2AX-TAT in younger BALB/c wild type (wt) mice (aged 66-76 days, n = 3) and older mice (aged 500-506 days, n = 3).

Separately, younger KPC mice (aged 66-77 days) without tumours (the lack of a tumour was confirmed on necropsy) were imaged by SPECT, 24 h after administration of ^{111}In-anti-γH2AX-TAT (n = 10) or ^{111}In-IgG-TAT (n = 8) as above. Survival of mice was followed for up to 64 days after SPECT imaging.

To evaluate the influence of an existing tumour on the uptake of ^{111}In-anti-γH2AX-TAT in KPC mice, imaging was performed 24 h after intravenous administration of ^{111}In-anti-γH2AX-TAT (n = 9) or ^{111}In-IgG-TAT (n = 7). Tumour presence was confirmed on necropsy (10 mice with tumour and 6 mice without).

To determine the influence of age on the distribution of ^{111}In-anti-γH2AX-TAT, three younger (aged 66-76 days) and three older Balb/c mice (aged 500-506 days) were intravenously injected with ^{111}In-anti-γH2AX-TAT.

Mice were euthanised by cervical dislocation and selected organs, tissues and blood were removed, and the percentage of the injected dose per gram (%ID/g) of each sample was calculated. Pancreatic tissue was flash-frozen with dry ice and stored at -80°C until required for further processing.

Autoradiography and Histological Analysis

Sections of pancreas tissue were exposed to a storage phosphor screen (PerkinElmer) to generate autoradiographs. The same *ex vivo* tissue sections were characterised by immunofluorescence, haematoxylin and eosin (H&E) and/or DAB (3,3′-Diaminobenzidine) staining to probe γH2AX expression and to determinine PanIN/PDAC status (as defined by Hruban et al. (*10*)). Morphological analysis was checked and endorsed by a qualified pathologist (RG). Full experimental details are provided in the Supplemental Information.

Statistical Analyses

All statistical and regression analyses were performed using GraphPad Prism v7 (GraphPad Software, San Diego, CA, USA). Linear regression with Runs test was used to check for correlations between measurements. After testing for normality using a Shapiro-Wilk test, means were compared using a t-test with Welch's correction for non-equal variances. One-way ANOVA tests followed by Dunnet's post-tests were used to compare multiple groups. Two-way ANOVA tests were used to analyse grouped data. All results are reported as mean ± standard deviation of at least three independent replicates, unless otherwise indicated.

RESULTS

γH2AX Is Upregulated during PDAC Development in KPC Mice

Using a set of pancreatic tissues obtained from KPC mice at different ages, we set out to investigate γH2AX expression during PDAC development. KPC mice exhibit invasive PDAC from 2 months of age onwards, with co-presentation of precursor lesions (*25*). Following histological classification of tissues, we confirmed the general relationship between PanIN presentation and age in our KPC mouse colony, with older animals presenting increasing amounts of all PanIN precursor lesions ($P < 0.0001$), including high-grade PanINs ($P = 0.0203$) (Supplemental Fig. 1A). Tumour formation in our colony occurred over a large interval with animals first showing FDG-avid lesions between 70 and 220 days of age. We observed no liver metastases in KPC mice in our colony.

We showed that this genetically engineered mouse model reproduces the hyperactivation of the DDR machinery observed in human PanINs and PDAC, as measured by γH2AX immunostaining (Fig. 1), first reported by Koorsta et al. (*18*), which themselves corroborated results from Bartkova et al. who showed DNA damage signalling hyperactivation in a large range of precursor lesions in other cancer sites (*15*). We observed little or no γH2AX staining in normal acinar tissue, in the earlier precursor lesions (PanIN-1), or in areas of marked lymphocyte infiltration; and little in PanIN-2 lesions and in regions of PDAC. However, there was marked γH2AX staining in all areas of high-grade precursor lesions (PanIN-3s). Previous reports showed very few cells expressing γH2AX foci in pancreata harvested from KC mice that only develop PanIN-1 and -2 lesions, since they lack the p53 mutation of KPC mice (*26*).

Since DNA laddering in the late stages of apoptosis also leads to pan-nuclear γH2AX expression, we evaluated apoptosis in sections of pancreata from KPC mice by staining for activated caspase-3 (Supplemental Fig. 2). Only in lymphocyte infiltrates, but not in PDAC or PanIN lesions was significant activated caspase-3 observed, suggesting that the γH2AX signal observed in PanIN-3 lesions is not a result of apoptosis.

In vivo Imaging of γH2AX in KPC Mice

In an effort to visualise this DDR activation in KPC mice in a non-invasive manner, we performed SPECT/CT imaging 24 h after intravenous administration of ^{111}In-anti-γH2AX-TAT (or the non-specific control, ^{111}In-IgG-TAT) to KPC mice of various ages. Mice that were administered ^{111}In-IgG-TAT yielded SPECT images that were consistent with the typical biodistribution of a radiolabelled antibody (Fig. 2, Supplemental Fig. 3).

In contrast, some younger and all older KPC mice that were administered ^{111}In-anti-γH2AX-TAT showed marked upper abdominal uptake, as well as the physiological signal observed in blood, heart, and liver as observed for ^{111}In-IgG-TAT (Fig. 2). Upper abdominal uptake of ^{111}In-anti-γH2AX-TAT was higher in older KPC mice. After removal of tissues from the mice, we quantified tracer uptake in a selected range of tissues (summarised in Supplemental Fig. 4). No age-related effects were seen after ^{111}In-IgG-TAT administration in any of the organs, including the pancreas ($R = 0.41$, $P>0.05$), indicating there were no non-target-specific or clearance-related effects. In contrast, after ^{111}In-anti-γH2AX-TAT administration a significant correlation of pancreatic uptake with age was revealed ($R = 0.83$, $P = 0.0015$) (4.7±0.92 vs. 6.6±0.56%ID/g in younger vs. older animals; $P = 0.0098$), but not in any of the other organs. This correlated with increased prevalence of PanIN3 lesions, reduced percentage of healthy pancreas,

and total increase in the relative area of PanIN lesions (Supplementaal Figs. 1B-D), and an increased uptake of ^{111}In-anti-γH2AX-TAT in the pancreas of tumour-bearing animals compared to non-tumour-bearing animals (where the presence or absence of a tumour was confirmed on necropsy; P = 0.015; Supplemental Fig. 5A). The biodistribution of ^{111}In-anti-γH2AX-TAT was not significantly different from that in age-matched wild-type BALB/c animals (aged 66-76 days; Supplemental Fig. 5B). In addition, we found no difference between organ uptake between younger and older BALB/c wild type animals (aged 50-506 days; P>0.05; Supplementa. Fig. 5), suggesting that the increase in ^{111}In-anti-γH2AX-TAT uptake in the pancreas was not merely related to ageing of the animals.

Given the different energies of the gamma-rays emitted by ^{111}In (171 and 245 keV) or ^{18}F (511 keV following annihilation of the positron emitted by the decaying radionuclide), we were able to image and quantify ^{111}In-anti-γH2AX-TAT and ^{18}F-FDG simultaneously (Fig. 2). In contrast to ^{111}In-anti-γH2AX-TAT imaging, we found no significant correlation between ^{18}F-FDG uptake in any of the organs with age, or PanIN stage (Supplemental Fig. 4C), corroborating earlier reports in human subjects where ^{18}F-FDG-PET imaging was of little utility for early detection of PDAC (*7,8*). Similarly, no difference was observed between total pancreatic uptake of ^{18}F-FDG in BALB/c animals versus KPC mice (P = 0.86; Supplemental Fig. 5B).

γH2AX Imaging in KPC Mice Correlates with Age and PanIN Stage

Assessment of ^{111}In-anti-γH2AX-TAT uptake in total pancreas of KPC mice, as measured by ex vivo gamma counting, revealed a clear correlation between the weight-normalized uptake of the tracer and the age of the mice (R = 0.83, P = 0.0015; Fig. 3), which in turn correlated with

PanIN extent ($P < 0.0001$; Supplemental Fig. 1A). This was not the case for the non-specific control compound ^{111}In-IgG-TAT ($R = 0.41$, $P = 0.32$).

Comparing the uptake of ^{111}In-anti-γH2AX-TAT in the pancreas with histological analysis, we found a trend towards correlation with the reduction in histologically normal pancreas tissue and increased uptake ($R = 0.69$, $P = 0.08$; Supplemental Fig. 1C). This trend was not observed for ^{111}In-IgG-TAT ($R = 0.058$, $P = 0.9$). In agreement with this, a clear correlation was also observed for the coverage of total PanIN lesions and pancreatic uptake of ^{111}In-anti-γH2AX-TAT ($R = 0.73$, $P = 0.031$), but not with ^{111}In-IgG-TAT ($R = 0.0015$, $P = 0.99$) (Supplemental Fig. 1D).

^{111}In-anti-γH2AX-TAT Is only Taken up in High-grade PanIN Lesions

To confirm that systemically delivered ^{111}In-anti-γH2AX-TAT co-localizes with high-grade PanIN lesions *in vivo*, we performed autoradiography and immunohistochemistry probing for γH2AX on sections of pancreatic tissue obtained from KPC mice (Fig. 4, additional sections shown as Supplemental Fig. 6). In line with our earlier results that γH2AX expression was mostly observed in high-grade PanIN-3 tissue, a significantly higher autoradiography signal was observed in high-grade PanIN-3s after administration of ^{111}In-anti-γH2AX-TAT, compared to normal pancreas, early PanIN lesions, lymphocyte infiltrates or PDAC, although some background uptake was observed in normal pancreas tissue. Quantitative analysis of autoradiographs following ^{111}In-anti-γH2AX-TAT imaging corroborated this observation, with high-grade PanIN lesions showing an uptake of the radiolabelled compound of 9.01 ± 0.72%ID/g versus 6.35 ± 0.51%ID/g for the total pancreas ($P<0.0001$), lymphocyte infiltrates ($P = 0.0001$), PanIN2 lesions ($P = 0.003$) or PDAC tissue ($P = 0.0073$) (Fig. 4F). No such correlation was observed in mice that were administered ^{111}In-IgG-TAT ($P>0.05$; Fig. 4G). Although we onserved a small increase in γH2AX

staining in PanIN2 lesions upon immunohistochemical analysis, this did not result in a significant increase of the uptake of ^{111}In-anti-γH2AX-TAT in these lesions, as measured by autoradiography ($P > 0.05$).

In addition, we observed no increased uptake of ^{111}In-anti-γH2AX-TAT in lymphocyte infiltrates, compared to normal pancreas ($P = 0.0001$). Furthermore, in a separate study, no increased uptake of ^{111}In-anti-γH2AX-TAT was measured in the pancreas of mice with caerulein-induced acute pancreatitis ($P>0.05$; Supplemental Fig. 7).

^{111}In-anti-γH2AX-TAT Uptake Predicts Onset of PDAC in KPC Mice

After showing that ^{111}In-anti-γH2AX-TAT is taken up preferentially in high-grade PanINs (i.e. PanIN-3s), and given that these lesions are regarded as direct precursors of PDAC, we evaluated, in a separate study, the ability of SPECT imaging with ^{111}In-anti-γH2AX-TAT to predict tumour formation and survival. KPC mice aged between 66-77 days were imaged by SPECT, 24 h after administration of ^{111}In-anti-γH2AX-TAT ($n = 11$) or control imaging agent ^{111}In-IgG-TAT ($n = 8$). Mice with increased uptake of ^{111}In-anti-γH2AX-TAT in the pancreas region (as indicated in Fig. 5A) survived significantly shorter than those with little discernible uptake (median survival 22 days vs. more than 63 days, respectively; $P = 0.0273$). No such observation was made in mice imaged with ^{111}In-IgG-TAT (all scans showed little to no uptake in the pancreas region, similar to Fig. 2C). All images obtained are shown in Supplemental Fig. 7. Mice were randomly assigned to ^{111}In-anti-γH2AX-TAT or ^{111}In-IgG-TAT imaging cohorts, which had no influence on survival ($P>0.05$; Supplemental Fig. 8). In addition, no correlation was found between the age at which these animals were imaged and their survival after the scan ($P>0.05$; Supplemental Fig. 8). Together with the observation that no increased uptake of ^{111}In-

anti-γH2AX-TAT is detected in age-matched wild-type mice (Supplemental Fig. 5B), our results suggest that visualising the high-grade PanIN-3 lesions using ^{111}In-anti-γH2AX-TAT can be used as an indicator of PDAC development in KPC mice. A caveat here is that of course all KPC mice will eventually grow tumours. The true specificity and selectivity of the method can therefore not be determined using the experimental setup in this proof-of-principle study.

In a separate study, we evaluated the effect of the presence or not of a tumour (confirmed on necropsy), on the uptake of ^{111}In-anti-γH2AX-TAT or the control compound ^{111}In-IgG-TAT. We observed increased uptake of ^{111}In-anti-γH2AX-TAT, but not ^{111}In-IgG-TAT in the whole pancreas in KPC mice bearing a tumour, compared to non-tumour-bearing animals ($P<0.05$; Fig. 5C), consistent with a higher PanIN-3 burden in resected pancreata of PDAC patients. None of the other organs showed significant differences in uptake ($P>0.05$; Supplemental Fig. 5B), apart from some non-consistent variation in kidney and spleen values.

DISCUSSION

Despite recent progress, there remains an urgent need for imaging methodologies for early detection of pancreatic ductal adenocarcinoma (*27,28*). Nearly a decade ago, Koorstra et al. described a hyperactivation of the DNA damage repair (DDR) machinery during PDAC development, with increasing expression of activated ATM (p(Ser1981)ATM), and its substrates pCHK2 and γH2AX in high-grade hyperplasias (PanIN-3 lesions) compared to normal tissue and low-grade PanINs, but less so in PDAC (*18*). This study was consistent with earlier data from Bartkova et al. who showed similar findings in a wide variety of other tumour types (*15*). Here, we confirmed that the KPC mouse model of PDAC replicates this biology, with a marked increase in γH2AX staining in PanIN-3 lesions. As in the human disease, DDR hyperactivation in KPC mice subsides in lesions reaching the PDAC stage. This offers the possibility to specifically visualise PanIN-3 precursor lesions, to complement currently employed imaging technologies, such as ultrasound, CT and MRI, that can only detect the later-stage, larger invasive PDAC lesions.

We demonstrate here that γH2AX imaging using ^{111}In-labelled, TAT-modified anti-γH2AX IgG can be used to detect high-grade PanINs *in vivo*, due to the propensity of these lesions to express higher levels of the phosphorylated γH2AX protein. Earlier studies had already shown that the ubiquitously used PET imaging agent ^{18}F-FDG does not allow clearly delineation of these precursor lesions (*24*). Although the differences in uptake of ^{111}In-anti-γH2AX-TAT described in PanIN3 vs. other tissues are subtle there is a clear benefit shown in survival studies. Our results here in a pancreatic cancer model confirm our earlier findings obtained in Balb/neuT mice, a genetically engineered mouse model of HER2-driven breast cancer (*20*). Notably, as before, no toxicity was observed from targeting an antibody to a DDR protein (*23*). Modelling showed previously that ^{111}In-anti-γH2AX-TAT caused no significant difference in DNA double strand

break (DSB) repair, or in clonogenic survival (*29*). On the other hand, we previously showed that, when increasing amount of ^{111}In were attached to anti-γH2AX-TAT (up to 6 MB/μg), the Auger electron emissions from ^{111}In could result in formation of additional DNA double strand break damage, and, consequently, more γH2AX foci, resulting in an autoamplificaiotn loop, and increased cell kill. A similar scenario may be proposed, where the DDR hyperactivation in pre-tumorous lesions is targeted by this therapeutic version of anti-γH2AX-TAT.

It is of note that we observed marked increases in total pancreatic uptake of ^{111}In-anti-γH2AX-TAT, where only a small portion of the pancreas is classed as diseased PanIN-3. In addition, we measured some signal in non-diseased pancreatic tissue in KPC mice, or in pancreas in naïve wild-type animals. This suggests that the uptake in the small PanIN-3 lesions is enough to enable macroscopic detection using the imaging agent. Importantly, it has been observed that, upon careful resection of whole pancreata, multiple advanced PanIN-3 lesions are the norm rather than the exception, and that PanINs are a disease that is able to spread through the entire ductal system (*12,13*), with densities of up to 0.16 lesions histologically detectable per cm^2 (*30*). This may aid detection in the clinical setting. Here, they may be used in conjunction with CT and MRI-based methods already in use for screening of high-risk patients, or aid as a guide for more invase sampling. In the former setting, the technology may also be used to further study the temporal relationship between PanIN3 burden and PDAC formation. In addition, detection of PanIN-3 burden may act as a prompt or a therapy efficacy readout for PanIN-3 ablation therapies.

Some of the limitations of our approach derive from the use of a whole antibody to target γH2AX. This makes it not only more difficult to produce than small molecule or peptide-based imaging vectors, but antibodies are generally slow to clear from blood circulation, and are taken up by the liver and spleen (*7*). This may limit the ability of any antibody-based imaging agent to

detect liver metastases. Nonetheless, the modified antibody we used here does afford an excellent selectivity and affinity (K_D = 23 nM) for its target epitope. Meanwhile, no other imaging vectors have yet been identified that reliably detect γH2AX, or any other post-translational modifications of phosphorylated serines and threonines that make up the bulk of information passed on in the DDR signalling networks.

Despite being well-characterised, γH2AX expression is mostly used in the context of DNA DSBs. However, γH2AX expression is not exclusively linked to DSBs, as it is also expressed around collapsed replication forks, and γH2AX expression can persist for hours or even days after any DSB have long since been repaired (*21*). Although it does raise a cautionary note for the interpretation of γH2AX imaging in general, this does not take away from its ability to act as a biomarker for pretumourous lesions, including PanIN-3s. It is also noteworthy that γH2AX expression is observed in the late stages of apoptosis, but we observed no correlation of apoptotic cells, as highlighted by activated caspase-3, with γH2AX staining or ^{111}In-anti-γH2AX-TAT uptake, perhaps aided by the short-lived nature of late apoptotic cells, causing only little contribution to the macroscopic signal observed by autoradiography or SPECT imaging. In addition, we observed no γH2AX-positive micronuclei resulting from genomic instability that may confound the detection of DDR upregulation by non-invasive imaging (*31*). Finally, it has been described that multiple links exist between DNA damage signalling and inflammatory signalling, and that DDR signalling influences immune surveillance of tumour tissue (*32*). Moreover, pancreatic inflammation is a key risk factor for pancreatic cancer (*33*), and this inflammation can directly affect epithelial cells to generate reactive oxygen and nitrogen species that lead to DNA damage and result in genetic instability. However, we observed no γH2AX staining in lymphocyte infiltrates in KPC mouse pancreata, suggesting that – at least in this setting – imaging of PanIN-

3s with ^{111}In-anti-γH2AX-TAT may be independent of immune cell presence. In addition, we observed no increased uptake in mice with caerulein-induced acute pancreatitis.

We have previously demonstrated that γH2AX imaging in PDAC can be used to detect DSB induction by cancer drugs or radiation (*34*). In clinical p ractice, this would enable early detection of treatment response, thereby allowing early switch to alternative therapies in non-responding patients. We now demonstrate that γH2AX imaging may allow early detection of pre-cancerous PanIN-3 precursor lesions. The data we present in this manuscript was obtained using a mouse model of PDAC only. Staining quantification we used here was distinct from the histo-scores used by Koorstra et al. (*18*). Although it mimics clinical tumorogenesis of PanINs to PDAC well, with similar γH2AX expression patterns, PET imaging with ^{89}Zr-anti-γH2AX-TAT in PDAC patients, and correlation between ex vivo autoradiography and PanIN histopathology is the next necessary step to validate this technology for human use.

In conclusion, we showed, for the first time, in a preclinical genetically engineered mouse model of PDAC, the possibility of imaging the hyperactivation of DNA damage repair signalling during pancreatic tumorigenesis, a direct result of genomic stress caused by oncogenic transformation. This novel tool may be used as a part of focussed surveillance in individuals at increased risk of developing PDAC.

ACKNOWLEDGEMENTS

This research was supported by CRUK through the Oxford Institute for Radiation Oncology and the CRUK Oxford Centre, the CRUK/EPSRC Imaging Centre in Oxford, and Pancreatic Cancer UK. JBT is funded through a project grant from the Pancreatic Cancer Research

Fund. Lastly, we wish to thank Professor Fergus Gleeson and Mr Paul Murphy at the Oxford University Hospitals NHS Foundation Trust for providing ^{18}F-FDG.

DISCLOSURE

The authors indicate that they have no potential conflicts of interest to report

KEY POINTS

Question: Can DNA Damage hyperactivation in pre-invasive cancer precursor lesions act as as means of early detection of pancreatic cancer by molecular imaging?

Pertinent Findings: In this study, we found that hyperactivation of DNA damage repair signalling in PanIN-3 lesions in a genetically engineered mouse model of spontaneous pancreatic ductal adenocarcinoma (PDAC) could be highlighted by molecular imaging, targeting γH2AX. This permitted to predict at an early stage which mice would develop PDAC.

Implications for patient care: This method may allow early detection of cancer in high-risk patient groups.

REFERENCES

1. Ferlay J, Soerjomataram I, Ervik M, et al. GLOBOCAN 2012 v1.0, Cancer Incidence and Mortality Worldwide: IARC CancerBase No. 11. http://globocan.iarc.fr]. Accessed 14/05, 2018.
2. Hidalgo M. Pancreatic cancer. New England Journal of Medicine. 2010;362:1605-1617.
3. Ansari D, Tingstedt B, Andersson B, et al. Pancreatic cancer: yesterday, today and tomorrow. Future Oncology. 2016;12:1929-1946.
4. Sohal DPS. Point: Weighing the risks and benefits of neoadjuvant therapy in resectable pancreatic cancer. Early, aggressive neoadjuvant therapy is appropriate in selected patients. Oncology (Williston Park). 2018;32:39-41, 44.
5. Zhang Q, Zeng L, Chen Y, et al. Pancreatic cancer epidemiology, detection, and management. Gastroenterology Research and Practice. 2016;2016:10.
6. Ballehaninna UK, Chamberlain RS. Serum CA 19-9 as a biomarker for pancreatic cancer—A comprehensive review. Indian Journal of Surgical Oncology. 2011;2:88-100.
7. England CG, Hernandez R, Eddine SBZ, Cai W. Molecular imaging of pancreatic cancer with antibodies. Molecular Pharmaceutics. 2016;13:8-24.
8. Strobel O, Buchler MW. Pancreatic cancer: FDG-PET is not useful in early pancreatic cancer diagnosis. Nat Rev Gastroenterol Hepatol. 2013;10:203-205.
9. Guo J, Xie K, Zheng S. Molecular biomarkers of pancreatic intraepithelial neoplasia and their implications in early diagnosis and therapeutic intervention of pancreatic cancer. Int J Biol Sci. 2016;12:292-301.
10. Hruban RH, Maitra A, Goggins M. Update on pancreatic intraepithelial neoplasia. Int J Clin Exp Pathol. 2008;1:306-316.
11. Shi C, Klein AP, Goggins M, et al. Increased prevalence of precursor pesions in familial pancreatic cancer patients. Clin Cancer Res. 2009;15:7737-7743.
12. Matsuda Y, Furukawa T, Yachida S, et al. The prevalence and clinicopathological characteristics of high-grade pancreatic intraepithelial neoplasia: Autopsy study evaluating the entire pancreatic parenchyma. Pancreas. 2017;46:658-664.
13. Makohon-Moore AP, Matsukuma K, Zhang M, et al. Precancerous neoplastic cells can move through the pancreatic ductal system. Nature. 2018;561:201-205.
14. Hruban RH, Goggins M, Parsons J, Kern SE. Progression model for pancreatic cancer. Clin Cancer Res. 2000;6:2969-2972.

15. Bartkova J, Hořejší Z, Koed K, et al. DNA damage response as a candidate anti-cancer barrier in early human tumorigenesis. Nature. 2005;434:864-870.
16. Halazonetis TD, Gorgoulis VG, Bartek J. An oncogene-induced DNA damage model for cancer development. Science. 2008;319:1352-1355.
17. Osterman M, Kathawa D, Liu D, et al. Elevated DNA damage response in pancreatic cancer. Histochemistry and Cell Biology. 2014;142:713-720.
18. Koorstra JBM, Hong SM, Shi C, et al. Widespread activation of the DNA damage response in human pancreatic intraepithelial neoplasia. Modern Pathology. 2009;22:1439-1445.
19. Cornelissen B, Kersemans V, Darbar S, et al. Imaging DNA damage in vivo using γH2AX-targeted immunoconjugates. Cancer Res. 2011;71:4539-4549.
20. Cornelissen B, Able S, Kartsonaki C, et al. Imaging DNA damage allows detection of preneoplasia in the BALB-neuT model of breast cancer. J Nucl Med. 2014;55:2026-2031.
21. Cornelissen B, Darbar S, Kersemans V, et al. Amplification of DNA damage by a γH2AX-targeted radiopharmaceutical. Nucl Med Biol. 2012;39:1142-1151.
22. Knight JC, Koustoulidou S, Cornelissen B. Imaging the DNA damage response with PET and SPECT. European Journal of Nuclear Medicine and Molecular Imaging. 2017;44:1065-1078.
23. Knight JC, Topping C, Mosley M, et al. PET imaging of DNA damage using (89)Zr-labelled anti-gammaH2AX-TAT immunoconjugates. Eur J Nucl Med Mol Imaging. 2015;42:1707-1717.
24. Serrao EM, Kettunen MI, Rodrigues TB, et al. MRI with hyperpolarised [1-13C]pyruvate detects advanced pancreatic preneoplasia prior to invasive disease in a mouse model. Gut. 2016;65:465-475.
25. Guerra C, Barbacid M. Genetically engineered mouse models of pancreatic adenocarcinoma. Mol Oncol. 2013;7:232-247.
26. Drosos Y, Escobar D, Chiang MY, et al. ATM-deficiency increases genomic instability and metastatic potential in a mouse model of pancreatic cancer. Sci Rep. 2017;7:11144.
27. Kramer-Marek G, Gore J, Korc M. Molecular imaging in pancreatic cancer--a roadmap for therapeutic decisions. Cancer Lett. 2013;341:132-138.
28. Yeh R, Steinman J, Luk L, Kluger MD, Hecht EM. Imaging of pancreatic cancer: what the surgeon wants to know. Clin Imaging. 2017;42:203-217.

29. Murray PJ, Cornelissen B, Vallis KA, Chapman SJ. DNA double-strand break repair: a theoretical framework and its application. J R Soc Interface. 2016;13:20150679.
30. Chatterjee D, Katz MH, Rashid A, et al. Pancreatic intraepithelial neoplasia and histological changes in non-neoplastic pancreas associated with neoadjuvant therapy in patients with pancreatic ductal adenocarcinoma. Histopathology. 2013;63:841-851.
31. Xu B, Sun Z, Liu Z, et al. Replication stress induces micronuclei comprising of aggregated DNA double-strand breaks. PLoS One. 2011;6:e18618.
32. O'Connor MJ. Targeting the DNA damage response in cancer. Mol Cell. 2015;60:547-560.
33. Farrow B, Evers BM. Inflammation and the development of pancreatic cancer. Surg Oncol. 2002;10:153-169.
34. Knight JC, Mosley MJ, Bravo LC, et al. (89)Zr-anti-gammaH2AX-TAT but not (18)F-FDG allows early monitoring of response to chemotherapy in a mouse model of pancreatic ductal adenocarcinoma. Clin Cancer Res. 2017;23:6498-6504.

FIGURES

Fig. 1

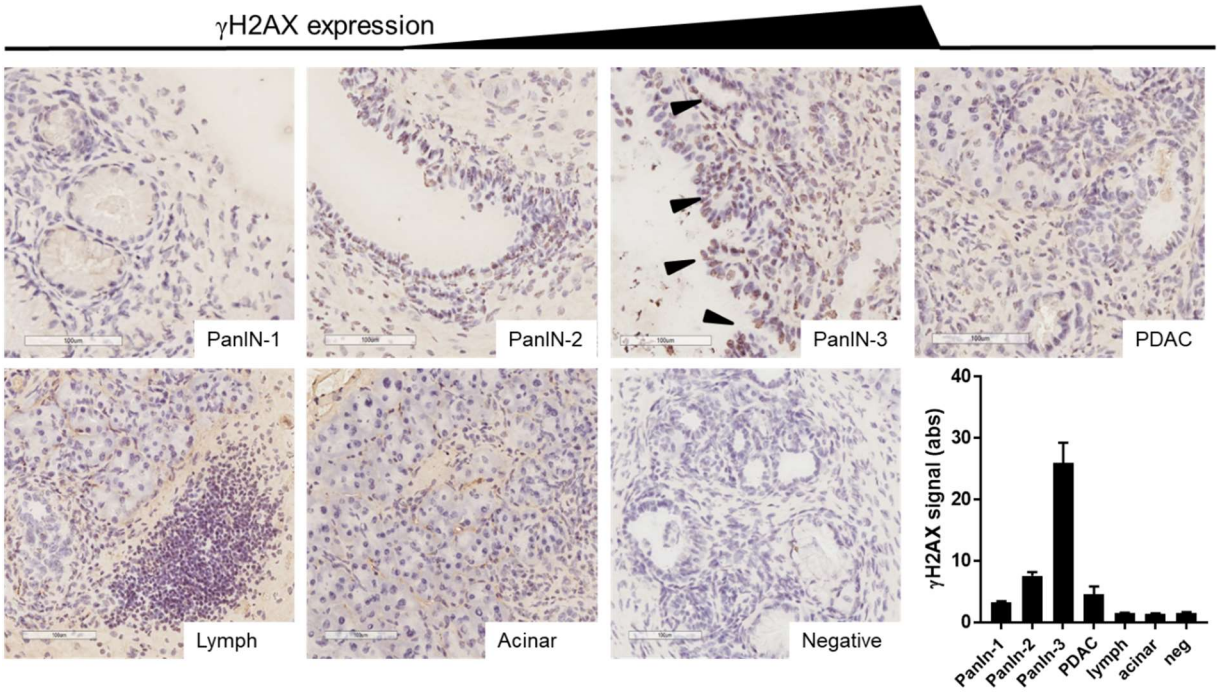

Fig. 1 Representative examples of γH2AX staining in various types of tissue in KPC mouse pancreata. (brown: γH2AX, purple: nuclei). Arrowheads indicate PanIN-3 lesions (Lymph: area of focal lymphocyte infiltration). Scale bar indicates 100 μm. The bottom right panel indicates semi-quantification of the intensity of staining (n = 12).

Fig. 2

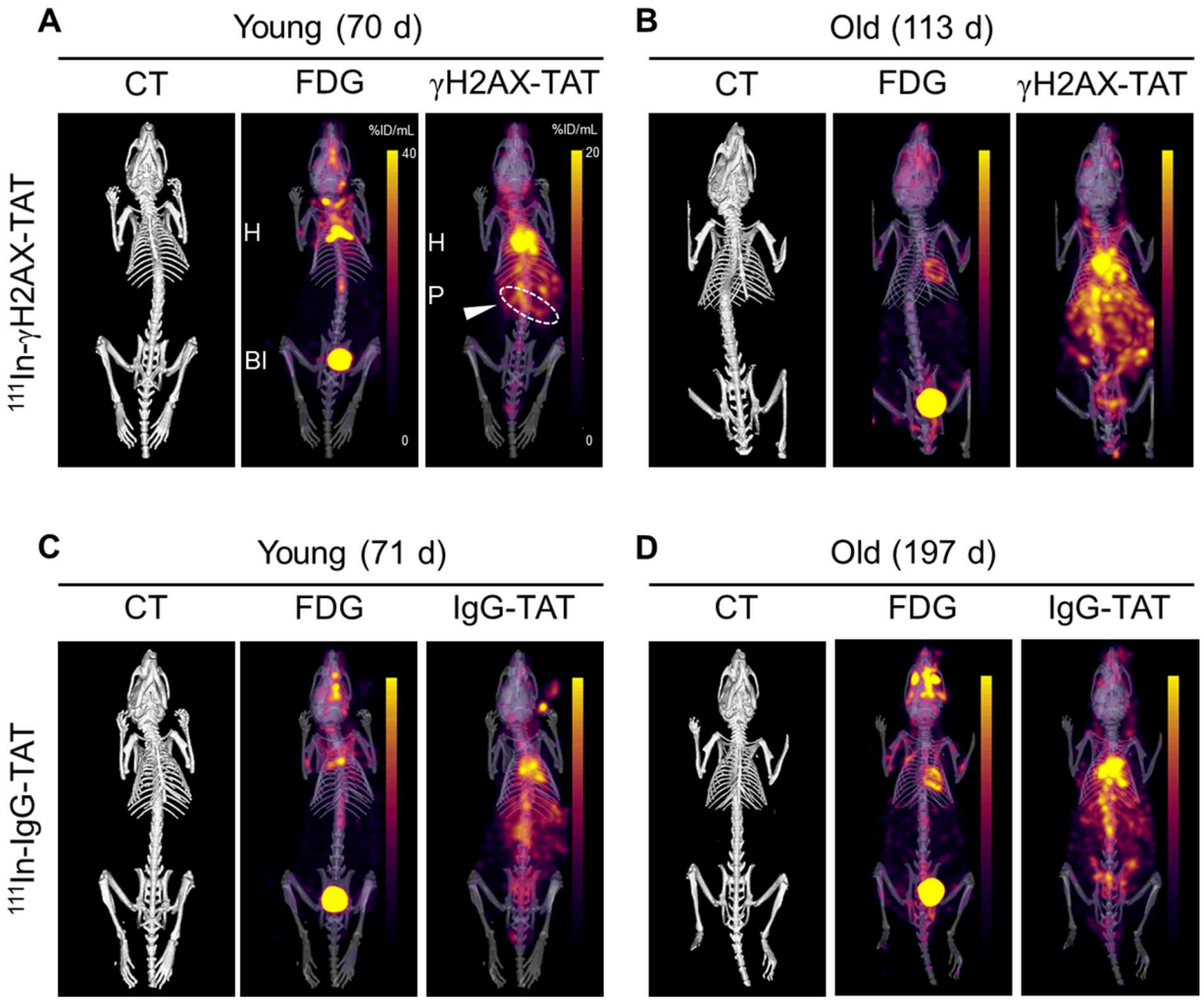

Fig. 2 Concurrently acquired ^{18}F-FDG, ^{111}In-anti-γH2AX-TAT (A, B) or ^{111}In-IgG-TAT (C, D), and CT images of KPC mice. Representative examples of either younger (A, C) or older animals (B, D) are presented. Image are shown as coronal MIPs, superimposed on a three-dimensional rendering of the CT image. Coronal images of the same mice are presented in Supplemental Fig. 3.

Fig. 3

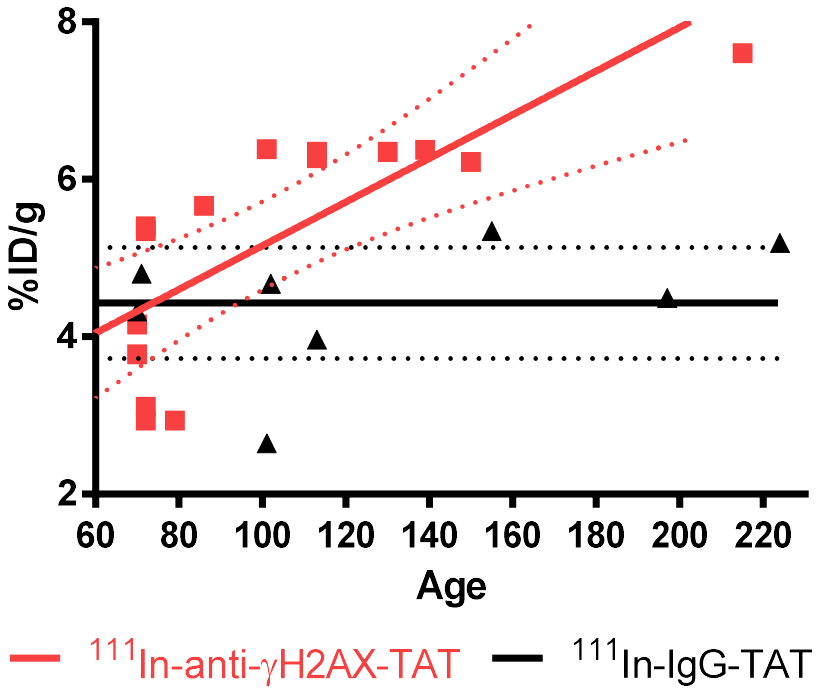

Fig. 3 *Ex vivo* biodistribution data showing uptake of ^{111}In in the pancreas of KPC mice versus age, after administration of either ^{111}In-anti-γH2AX-TAT or ^{111}In-anti-RIgG-TAT (5 MBq, 5 μg). Linear regression analysis showed no significant correlation of IgG control compound with age, but an increase of ^{111}In-anti-γH2AX-TAT with age, corresponding to the increased hyperplastic high-grade PanIN load in these animals.

Fig. 4

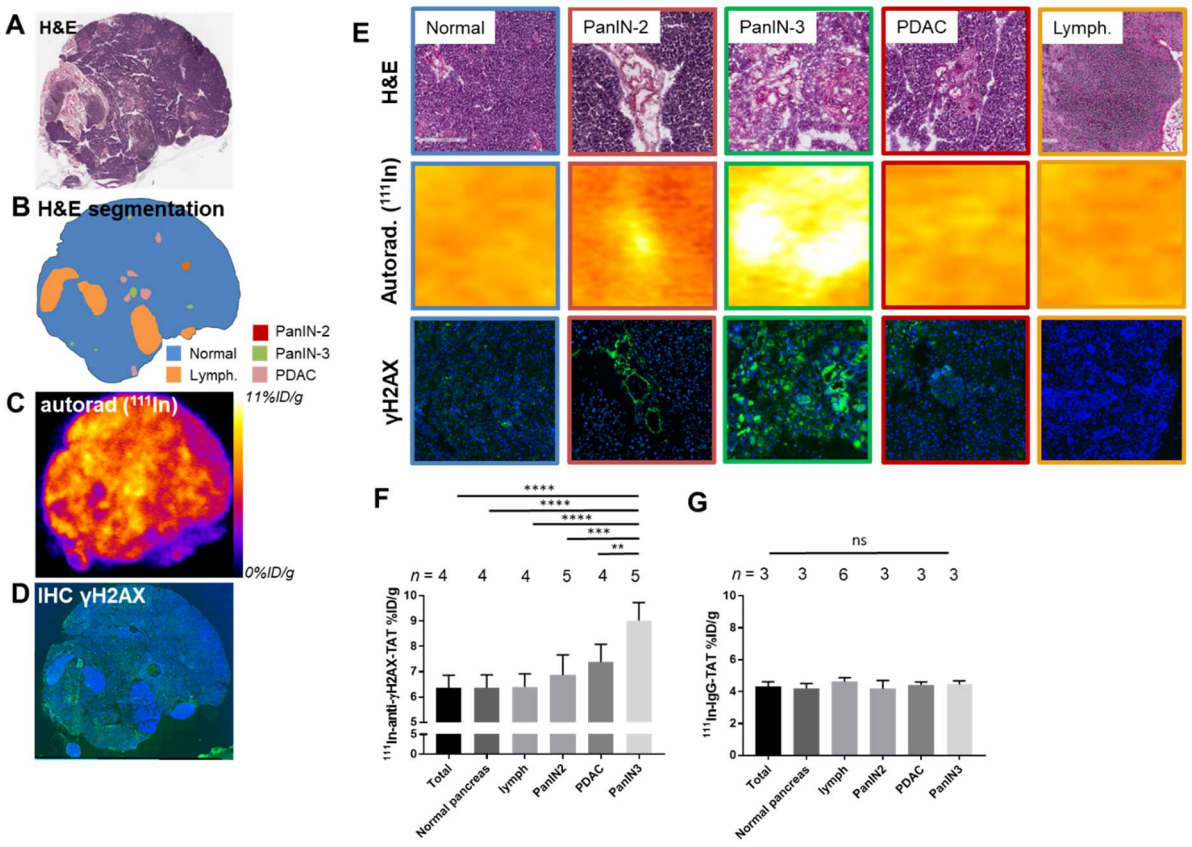

Fig. 4 (A) H&E staining of a pancreas section from a 113-day old KPC mouse harvested 24 h post-administration of ^{111}In-anti-γH2AX-TAT, (B) identification of the various morpho-pathological features (Lymph. = Lymphocytes), (C) autoradiography image showing the distribution of radioactivity, and (D) immunofluorescence image showing γH2AX (green) and nuclei (blue). Additional sections are shown in Supplemental Fig. 6. (E) maginifacitons of histological areas in A-D. (F) Uptake of ^{111}In-anti-γH2AX-TAT in various morpho-pathological features in KPC pancreata, measured by ex vivo autoradiography of pancreas sections. (G) Uptake of ^{111}In-IgG-TAT in various morpho-pathological features in KPC pancreata, measured by ex vivo autoradiography of pancreas sections.

Fig. 5

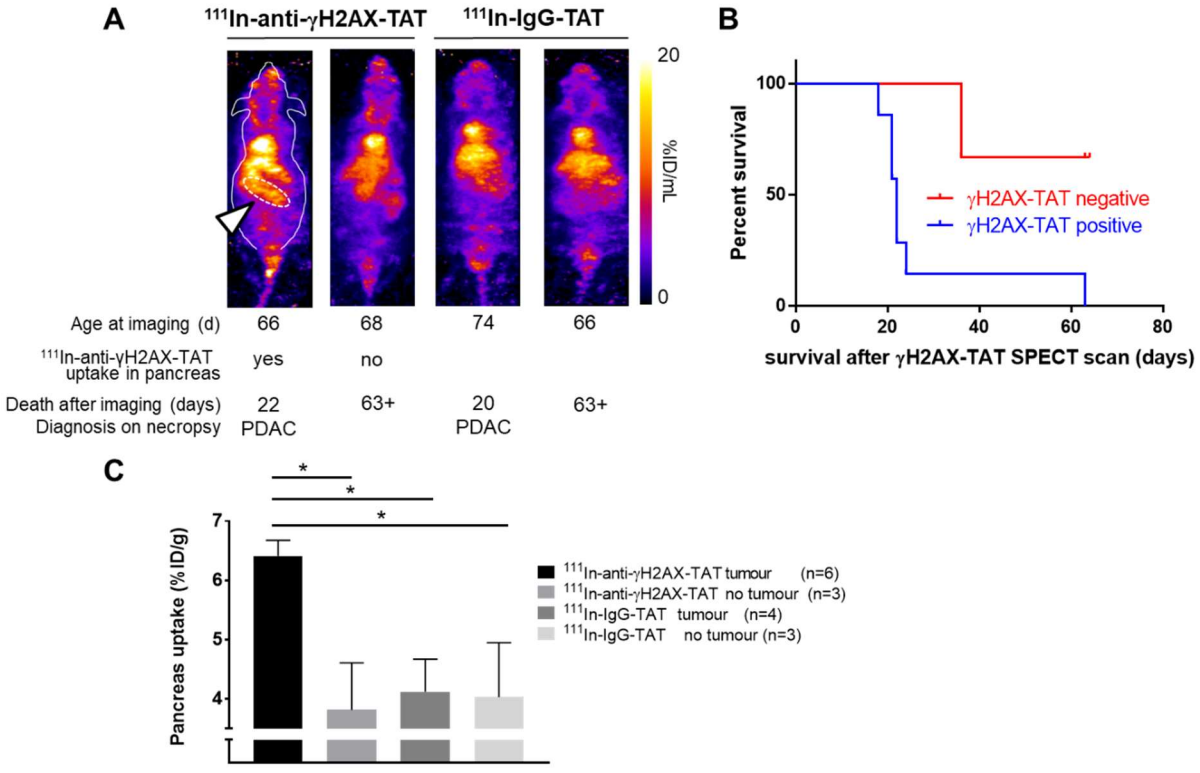

Fig. 5 (A) Representative images of KPC mice aged between 66-77 days imaged by SPECT, 24 h after intravenous administration of ^{111}In-anti-γH2AX-TAT. Age at the time of imaging, the length of survival before clinical symptom endpoints were reached, and the diagnosis at necropsy are indicated for each mouse. The pancreatic region is indicated by the white arrowhead and white dashed line in the first animal only. (Coronal MIPs are shown, an outline of a mouse is indicated for the first animal only). (B) Mice showing uptake of ^{111}In-anti-γH2AX-TAT in the pancreas showed significantly shorter survival than those not showing pancreatic uptake (P = 0.0273). (C) ^{111}In-anti-γH2AX-TAT, but not ^{111}In-IgG-TAT, is taken up more in pancreata of tumour-bearing KPC mice.

Supporting information for

Early Detection in a Mouse Model of Pancreatic Cancer by Imaging DNA Damage Response Signalling

James C. Knight[1,2], Julia Baguña Torres[1], Robert Goldin[3], Michael Mosley[1], Gemma M. Dias[1], Luisa Contreras Bravo[1], Veerle Kersemans[1], P. Danny Allen[1], Somnath Mukherjee[1], Sean Smart[1], and Bart Cornelissen[1†]

[1] CR-UK/MRC Oxford Institute for Radiation Oncology, Department of Oncology, University of Oxford, Oxford, United Kingdom

[2] School of Natural and Environmental Sciences, Newcastle University, Newcastle upon Tyne, United Kingdom

[3] Department of Histopathology, Imperial College London, St Mary's Hospital Campus, London, United Kingdom

Supplemental Methods

PET/SPECT/CT Imaging

General

PET/SPECT/CT imaging was performed using a VECTor^4 imaging system (MILabs) using a rat collimator with 1.8 mm pinholes. List-mode PET/SPECT data were acquired for 30 minutes and a CT image was then subsequently acquired (55 kV, 0.19 mA) on the same system. For the indium-111 SPECT images, reconstructions were performed using a γ-ray energy window of 156–190 keV (background weight 2.5), 0.6 mm^3 voxels, 128 subsets, and 2 iterations using the manufacturer's POSEM reconstruction protocol. For the fluorine-18 PET images, reconstructions were performed using energy windows of 460-562 keV (background weight 2.5), 0.8 mm^3 voxels, 128 subsets, and 5 iterations using the manufacturer's POSEM reconstruction type. To allow accurate scaling and quantification, calibration factors (determined from phantoms) were applied to the data. PET and SPECT images were each registered to CT and then attenuation corrected. During each imaging

session, mice were kept under anaesthesia by inhalation of 2% isofluorane in air and maintained at 37°C. Images were processed and volume-of-interest analyses were performed using the PMod software package (version 3.807, PMOD Technologies).

^{111}In-anti-γH2AX-TAT and ^{18}F-FDG imaging in ageing KPC mice

At various ages (ranging from 70 to 224 days), KPC mice underwent dual-isotope (^{18}F and ^{111}In) PET/SPECT imaging at 1 h after administration of ^{18}F-FDG, and at 24 h after injection of either ^{111}In-anti-γH2AX-TAT (n = 9) or ^{111}In-anti-IgG-TAT (n = 8). After imaging, selected tissues and blood were harvested, and the percentage of the injected dose of radiolabelled compound per gram in each of them was determined. Pancreatic tissue was snap-frozen, cyrosectioned, and processed for autoradiography, γH2AX immunohistochemistry and haematoxylin and eosin (H&E) staining.

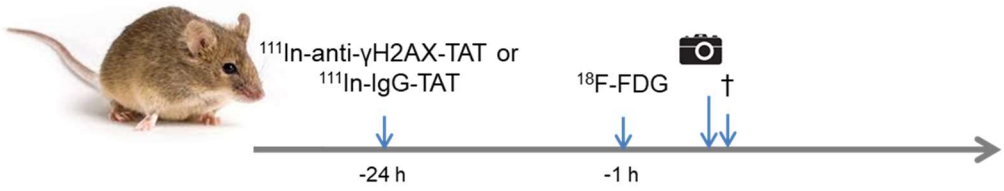

^{111}In-anti-γH2AX-TAT imaging and survival in KPC mice

KPC mice (aged 66-77 days) without tumours were imaged by SPECT, 24 h after administration of ^{111}In-anti-γH2AX-TAT (n = 10) or ^{111}In-IgG-TAT (n = 8) as above. Survival of mice was followed for up to 64 days after SPECT imaging. Mice were euthanised when they showed the first clinical symptoms of disease. Diagnosis of PDAC was confirmed on necropsy.

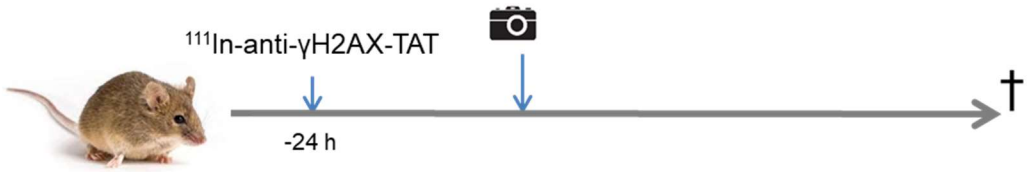

^{111}In-anti-γH2AX-TAT imaging in tumour-bearing KPC mice

To evaluate the influence of an existing tumour on the uptake ^{111}In-anti-γH2AX-TAT in KPC mice, animals were euthanised 24 h after intravenous administration of ^{111}In-anti-γH2AX-TAT (n = 9) or ^{111}In-IgG-TAT (n = 7). Selected organs and tissues were harvested and the percentage of the injected dose per gram of tissue was determined. Pancreata were measured with the tumour(s) if present. Tumour presence was confirmed on necropsy (10 mice with tumour and 6 mice without tumour were included in this study).

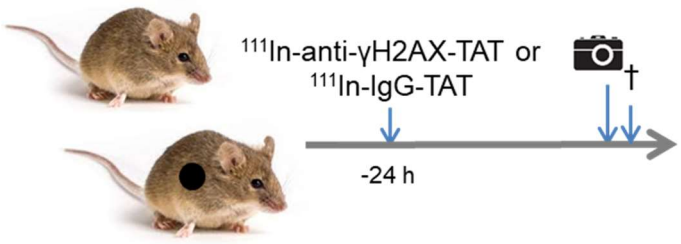

^{111}In-anti-γH2AX-TAT imaging in older wild type mice

To determine the influence of age on the distribution of ^{111}In-anti-γH2AX-TAT, three younger (aged 66-76 days) and three older (aged 500-506 days) mice were intravenously injected with ^{111}In-anti-γH2AX-TAT. 24 h later, selected organs and blood were harvested and the percentage of the injected dose per gram of tissue was determined.

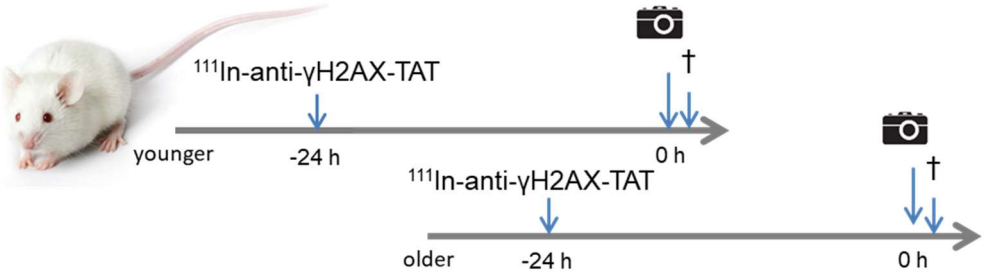

^{111}In-anti-γH2AX-TAT imaging in mice with acute pancreatitits

Caerulein, sulfated (MPBIO, UK) was dissolved in 0.9 % saline for an injectable dose of 50 ug/kg in 30 µL. C57BL/6 female mice, 10 weeks of age were injected (IP) with either caerulein or saline

over a period of 6 hours. At 7.5 hours post the initial caerulein or saline injection all mice were injected via the tail vein with ^{111}In-DTPA-γH2Ax-TAT (4.5 MBq, 5ug).

SPECT/CT images were acquired 24 h later, for approximately 30 min using a VECTor^{4}CT scanner (MILabs, Utrecht, the Netherlands) as above. Immediately after imaging, mice were euthanised by cervical dislocation and selected organs, tissues and blood were removed. The samples were immediately rinsed with water, dried, and transferred into a pre-weighed counting tube. After weighing the filled counting tubes, the amount of radioactivity in each was measured using a HiDex gamma counter (Lablogic). Counts per minute were converted into radioactivity units (MBq) using calibration curves generated from known standards. These values were decay-corrected to the time of injection, and the percentage of the injected dose per gram (%ID/g) of each sample was calculated. Pancreatic tissue was flash-frozen with dry ice and stored at -80°C until required for further processing.

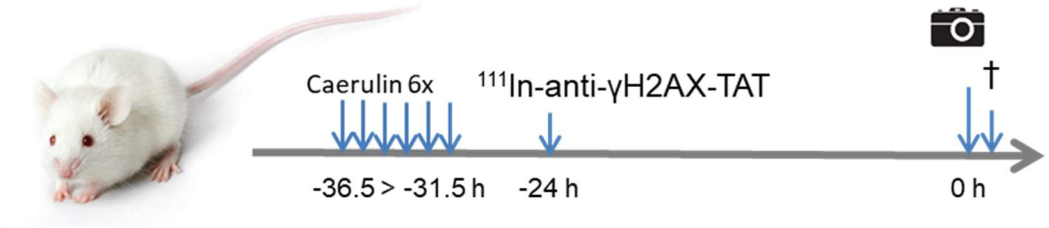

***Ex vivo* biodistribution experiments**

After imaging (unless long-term follow-up was necessary), mice were euthanised by cervical dislocation and selected organs, tissues and blood were removed. The samples were immediately rinsed with water, dried, and transferred into a pre-weighed counting tube. After weighing the filled counting tubes, the amount of radioactivity in each was measured using a 2480 WIZARD^2 (PerkinElmer) or HiDex gamma counter (Lablogic). Counts per minute were converted into radioactivity units (MBq) using calibration curves generated from known standards. These values were decay-corrected to the time of injection, and the percentage of the injected dose per gram (%ID/g) of each sample was calculated. Pancreatic tissue was flash-frozen with dry ice and stored at -80°C until required for further processing.

Immunofluorescence Imaging

Pancreases harvested from mice (n = 12) were flash frozen and 8 μm sections were prepared using a cryostat. Sections were stored at -80°C until use. Slides were allowed to reach room temperature for 10 minutes then washed briefly in phosphate-buffered saline (PBS) pH 7.4. The slides were fixed in 4% paraformaldehyde/PBS for 10 min, then washed three times in PBS for 5 min. Sections were permeabilized in 1% Triton X-100 for 10 min, washed, and non-specific binding was blocked by incubation of the slides in 2% BSA/PBS + 0.1% Triton X-100 for 1 h at 37°C. Slides were briefly allowed to dry and each section was isolated using a PAP pen. To each appropriate section approximately 100 μL of primary anti-γH2AX monoclonal antibody (Merck, catalogue no. 05-636, clone JBW301) diluted 1:250 in 2% BSA/PBS + 0.1% Triton X-100, or just 2% BSA/PBS + 0.1% Triton X-100, was applied, and incubated for 1 h at 37°C. The slides were washed three times in PBS for 5 min and the secondary goat anti-mouse Alexa Fluor-488 antibody (ThermoFisher Scientific, catalogue no. A-11001) diluted 1:250 in 2% BSA/PBS was applied and incubated for 1 h at 37°C. The slides were then washed in PBS, excess fluid removed, mounted using Vectashield containing DAPI (Vector Laboratories, catalogue no. H-1200). Slides were stored at 4°C in the dark. Images were acquired using a Leica SP8 confocal fluorescent microscope.

Autoradiography

Sections of pancreas tissue were exposed to a storage phosphor screen (PerkinElmer) to generate autoradiographs. Quantification was performed in one section each from at least three animals (as indicated) by ImageJ, using regions-of-interest based on H&E-based morpho-pathological features. The average intensity per VOI was used as a metric, and converted to %ID/g using known standards.

3,3'-Diaminobenzidine (DAB) and Haematoxylin Staining

To prevent staining of endogenous peroxidases, pancreas sections were incubated with 1.5% H_2O_2 for 15 minutes at room temperature and then rinsed with deionised water. Slides were briefly allowed to dry and each section was isolated using a PAP pen. Non-specific binding was blocked by incubation of the slides in 5% goat serum in PBS + 0.1% Tween-20 for 1 h at 37°C. To each section approximately 100 μL of primary anti-γH2AX monoclonal antibody (Merck, catalogue no.

05-636, clone JBW301) diluted 1:800 in 5% goat serum in PBS + 0.1% Tween-20, or just 5% goat serum in PBS + 0.1% Tween-20, was applied, and incubated for 1h at room temperature. The slides were washed three times in PBS for 5 min and the secondary goat anti-mouse antibody (BA-9200, Vector Laboratories) diluted 1:250 in 5% goat serum in PBS + 0.1% Tween-20 was applied and incubated for 30 minutes at room temperature. The slides were then washed three times in PBS + 0.1% Tween-20 for 5 minutes. ABC-HRP (Vactastain Elite, ABC-HRP reagent, R.T.U. peroxidase, PK-7100) was then applied to each section and incubated for 30 minutes at room temperature. The slides were then washed three times in PBS + 0.1% Tween-20 for 5 minutes. DAB solution (Pierce, DAB substrate kit) was then applied to each section and incubated for 5 minutes. The slides were then washed three times with deionised water for 5 min and then counterstained with haematoxylin for 2 minutes. Slides were washed in running tap water and then dehydrated with an increasing concentration gradient of ethanol. Slides were mounted using DPX mounting medium and then stored at 4°C in the dark. Images were acquired at a 20x magnification using an Aperio Slide Scanner (Leica Biosystems) and analysed using the Aperio ImageScope Viewer (Leica Biosystems).

Supplemental Fig. 1

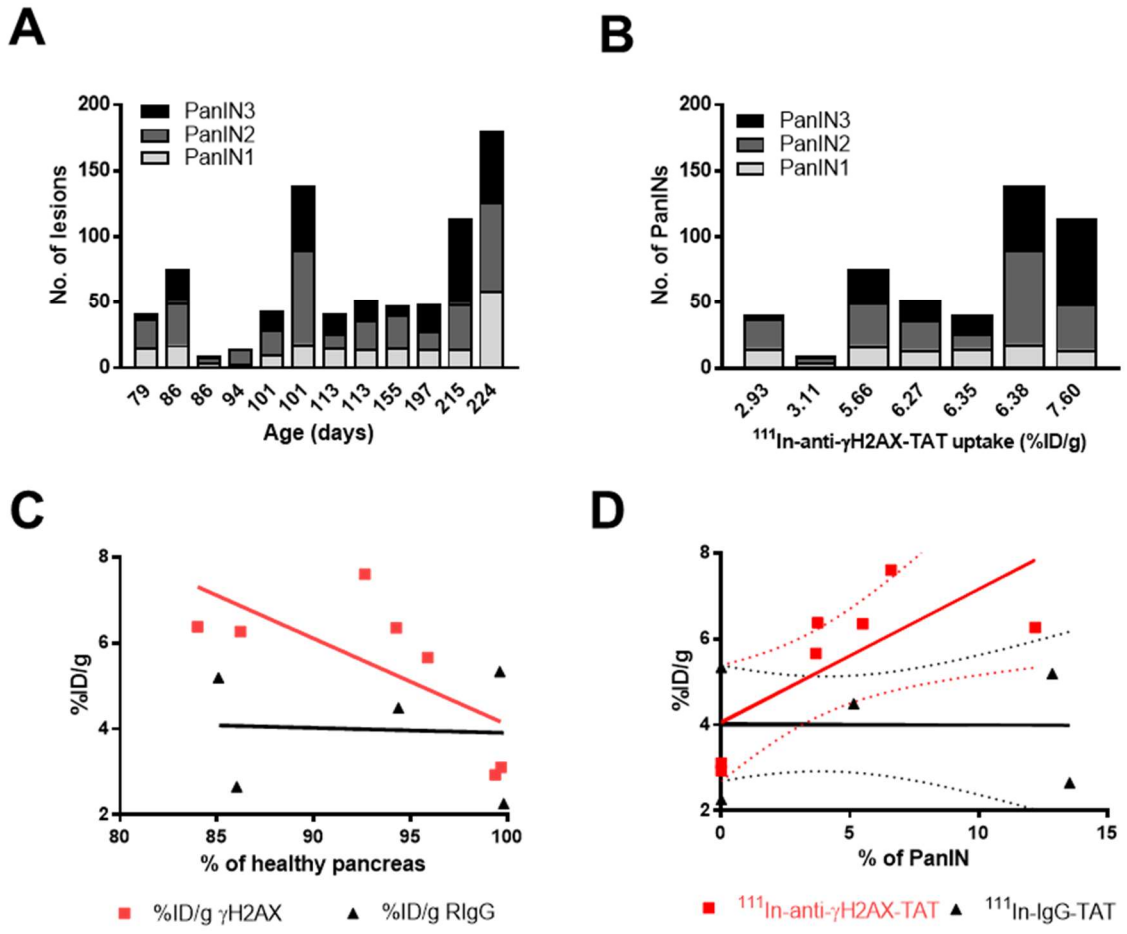

Supplemental Fig. 1 (A) Quantification of the extent of PanIN1, 2, and 3 involvement in KPC mice of varying ages shows a clear correlation of PanIN3 presentation with age (n = 12). (B) Consistent with higher γH2AX expression in PanIN3 lesions, uptake of ^{111}In-γH2AX-TAT in pancreata of KPC mice correlates with the amount of PanIN3 lesions (n = 7). (C) Similarly, uptake of ^{111}In-anti-γH2AX-TAT, but not ^{111}In-IgG-TAT, in KPC mouse pancreas decreases with an increasing amount of healthy pancreatic tissue (n = 7 and 5, respectively). (D) Corroborating these observations, there is a trend towards a correlation between the extent of PanIn3 lesions and ^{111}In-γH2AX-TAT uptake in KPC mouse pancreas (n = 7 and 5, respectively).

Supplemental Fig. 2

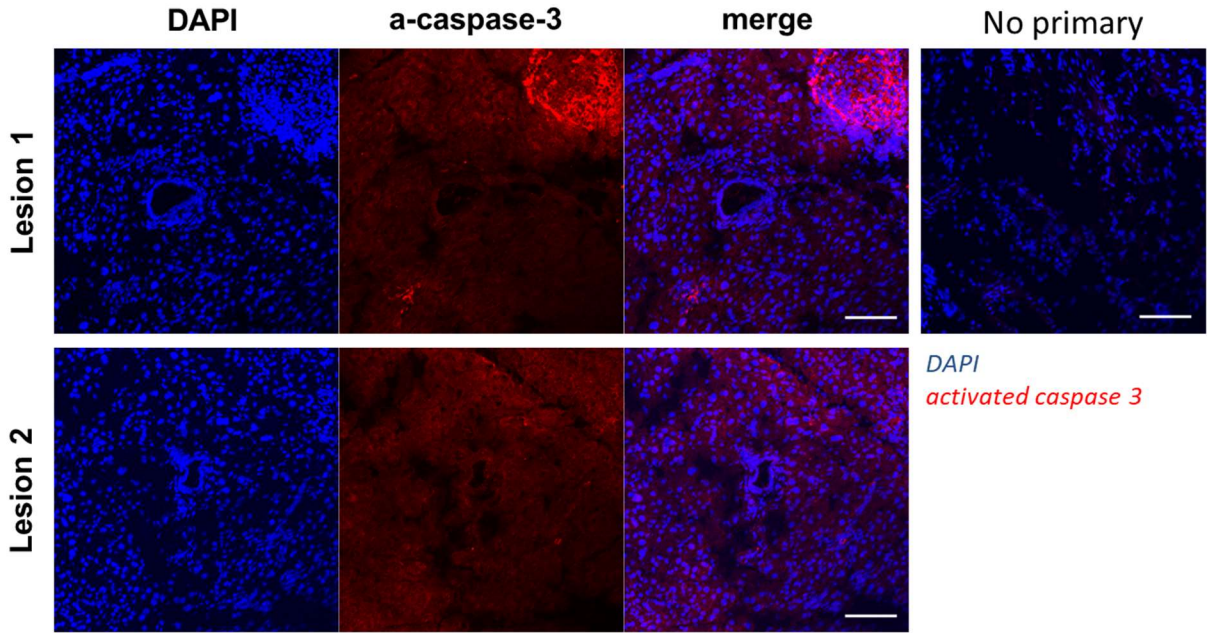

Supplemental Fig. 2 Activated caspase-3 staining in KPC mouse pancreas sections reveals little to no caspase activation in two independent PanIN3 lesions. No correlation with tissue positive for γH2AX were observed. Scale bar indicates 50 μm. A negative control where the primary anti-capsase-3 antibody was omitted is also included to demonstrate the lack of non-specific staining or autofluorescence.

Supplemental Fig. 3

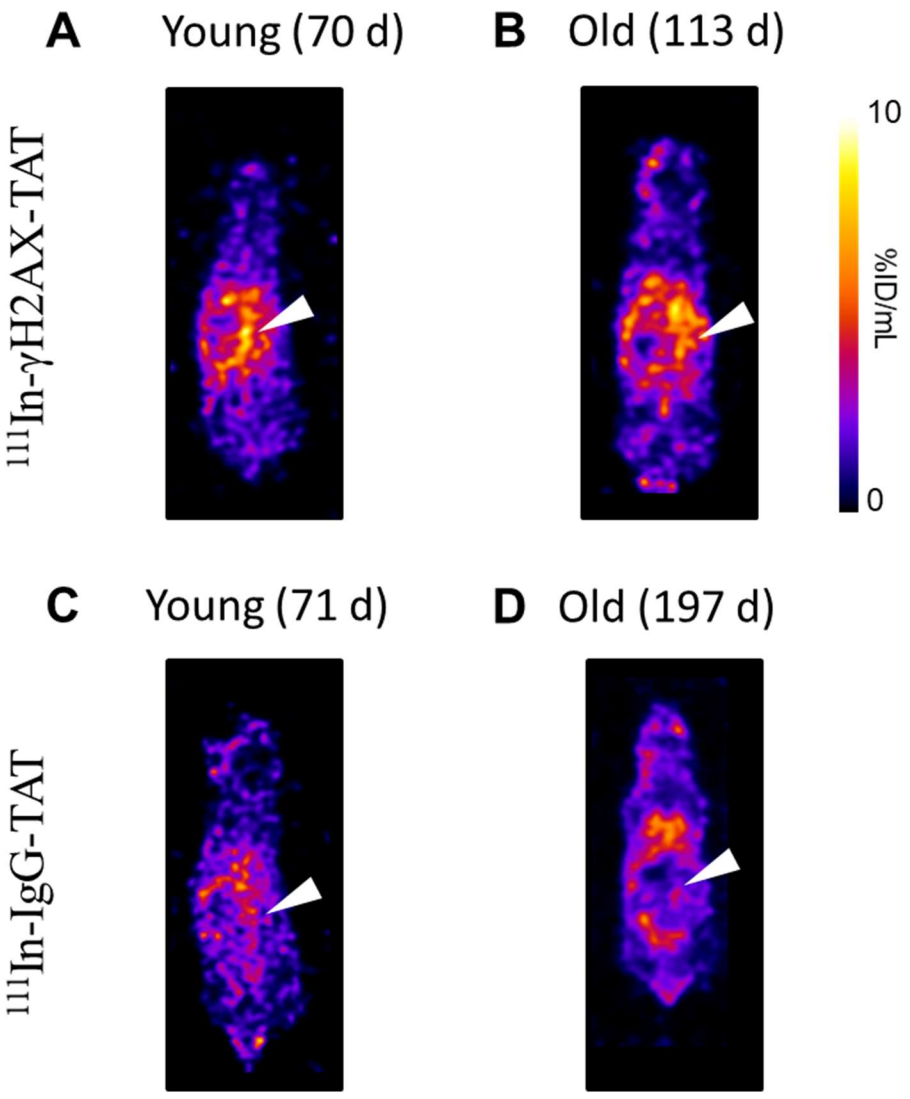

Supplemental Fig. 3: ^{111}In-anti-γH2AX-TAT (A, B) or ^{111}In-IgG-TAT (C, D) imaging in KPC mice. Representative examples of either younger (A, C) or older animals (B, D) are presented. Image are shown as coronal sections through the pancreas (indicated by the white arrowhead).

Supplemental Fig. 4

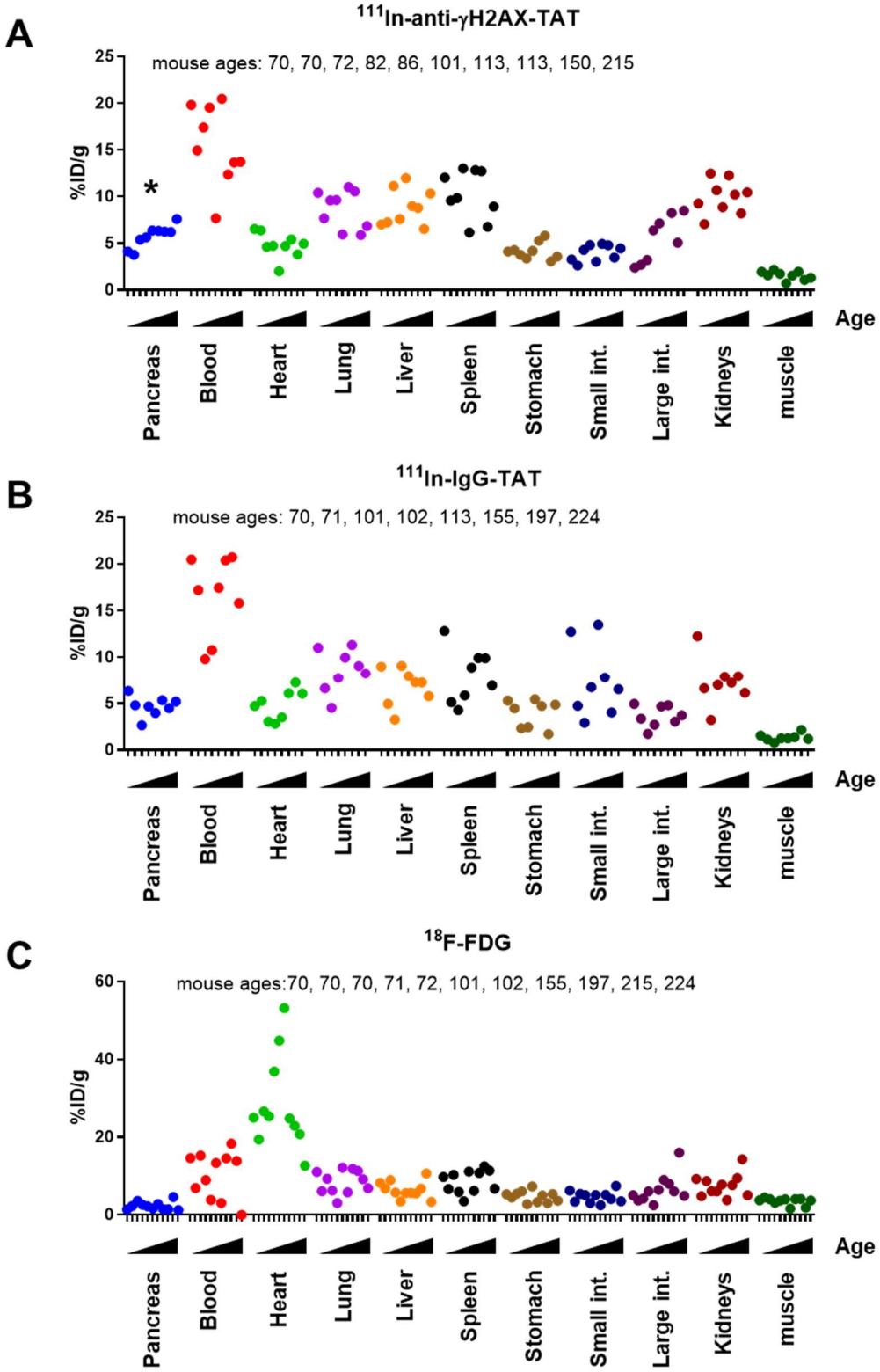

Supplemental Fig. 4 *Biodistribution of ^{111}In-anti-γH2AX-TAT (A), ^{111}In-IgG-TAT (B), or ^{18}F-FDG (C) in KPC animals of various ages. Results are expressed as the percentage of the injected dose per gram of tissue. (* significant correlation of %ID/g with age)*

Supplemental Fig. 5

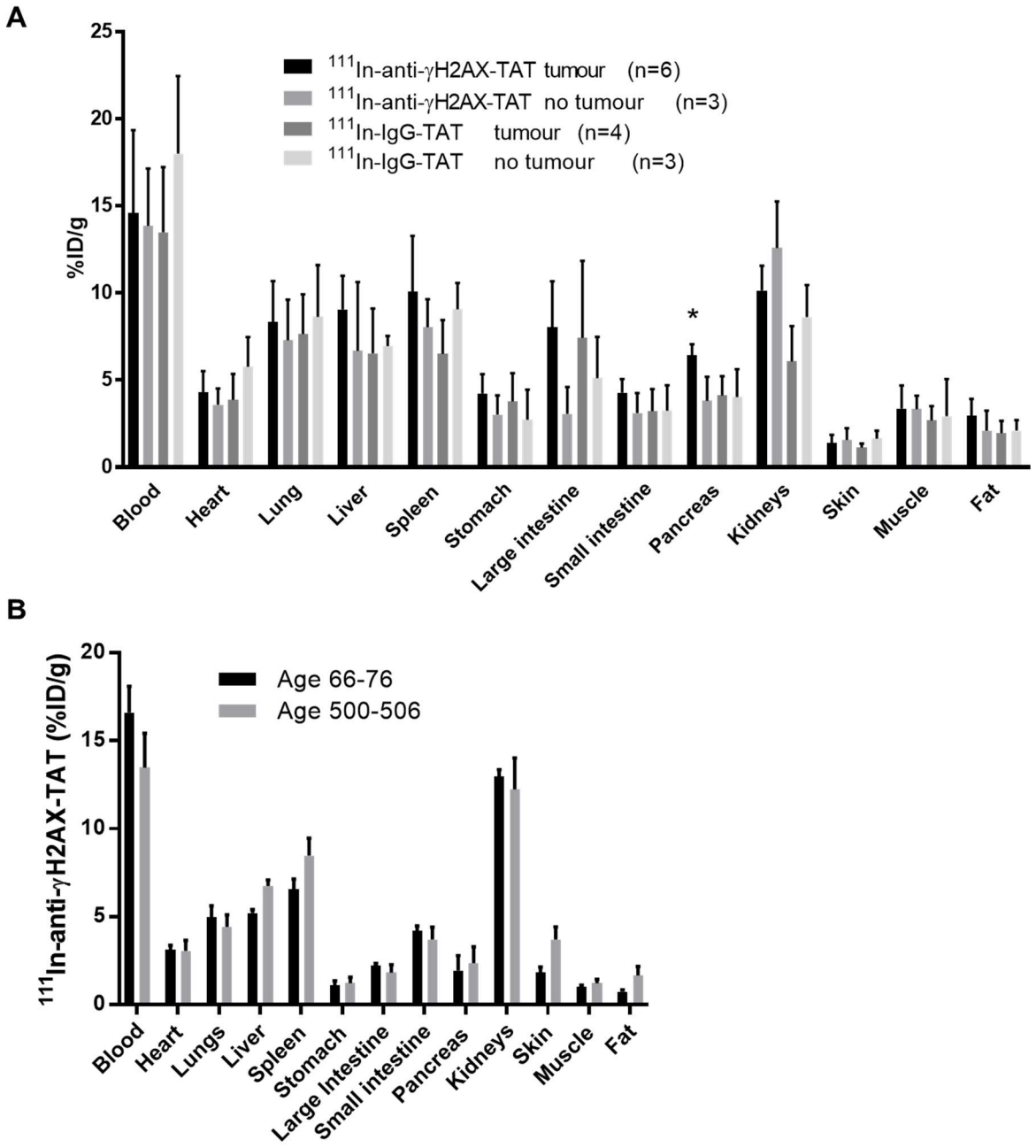

Supplemental Fig. 5 (A) ^{111}In-anti-γH2AX-TAT, but not ^{111}In-IgG-TAT, is taken up more in pancreata of tumour-bearing KPC mice. The pressence of a tumour or lack thereof was confirmed on necropsy. (P = 0.015) (B) The biodistribution of ^{111}In-anti-γH2AX-TAT is not significantly different in older Balb/c wild type animals compared to younger mice.*

Supplemental Fig. 6

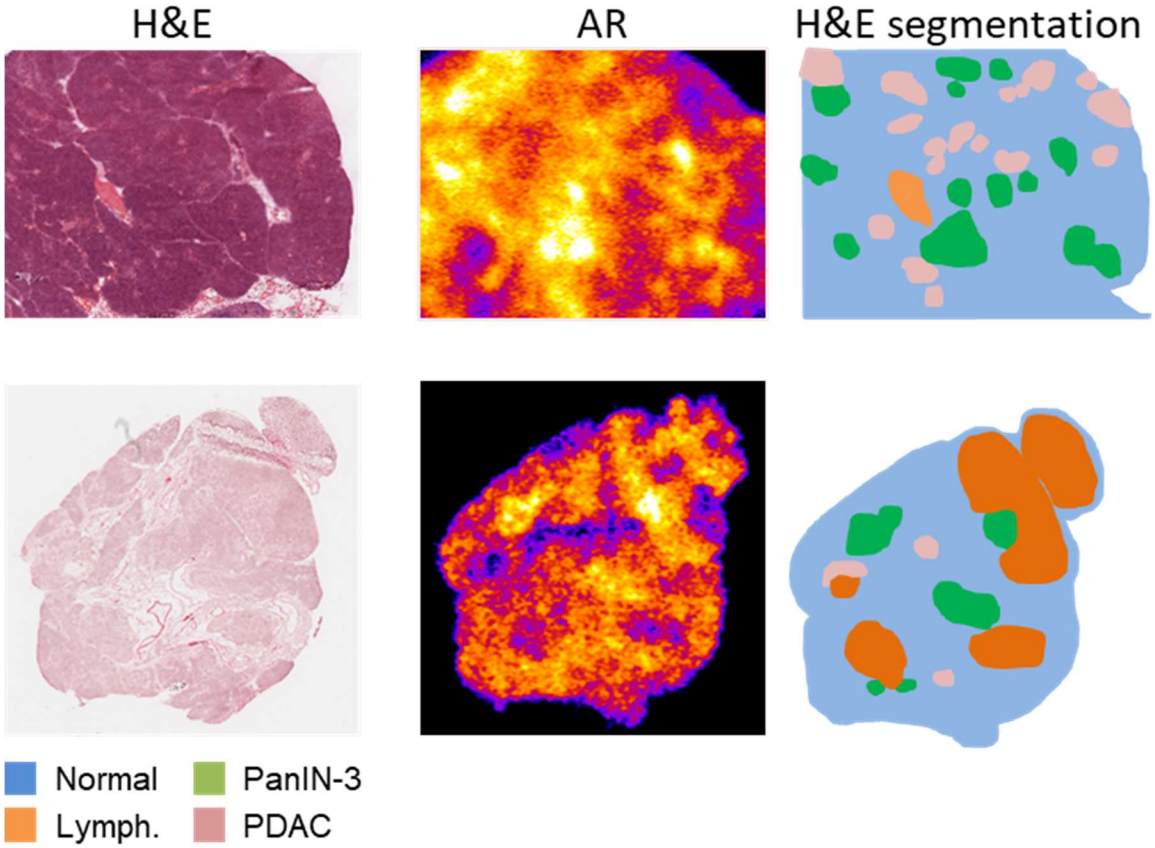

Supplemental Fig. 6. As in Figure 4 A-C. Additional sections.

Supplemental Fig. 7

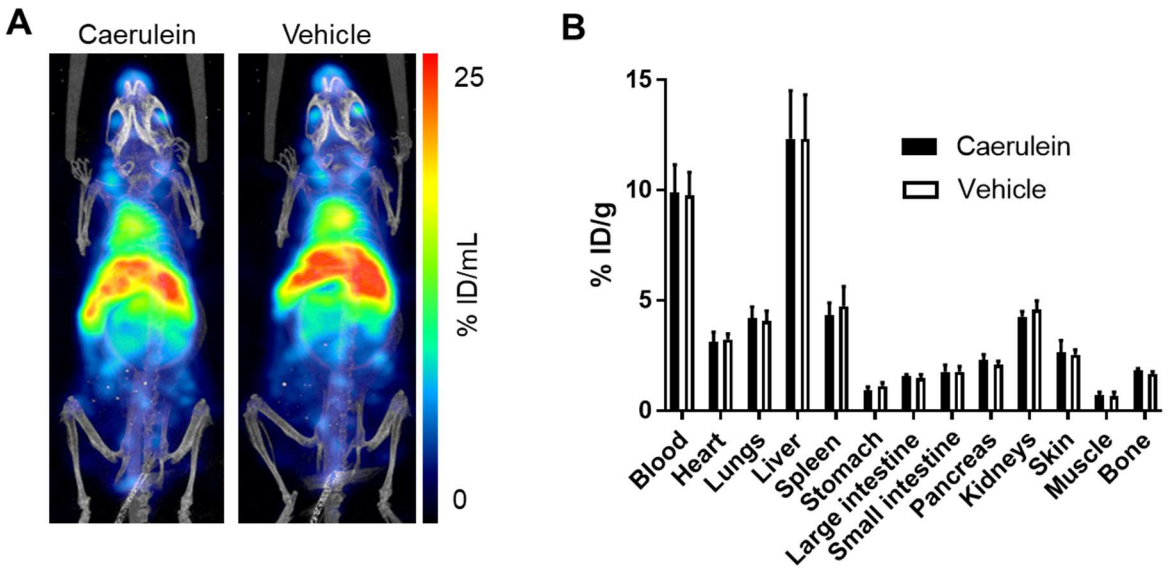

Supplemental Fig. 7 (A) Representative SPECT/CT images of Balb/c mice, treated with caerulein or vehicle control, and imaged 24 h after administration of ^{111}In-anti-γH2AX-TAT (5 MBq/μg) (B) Ex vivo biodistribution results follwing imaging in A.

Supplemental Fig. 8

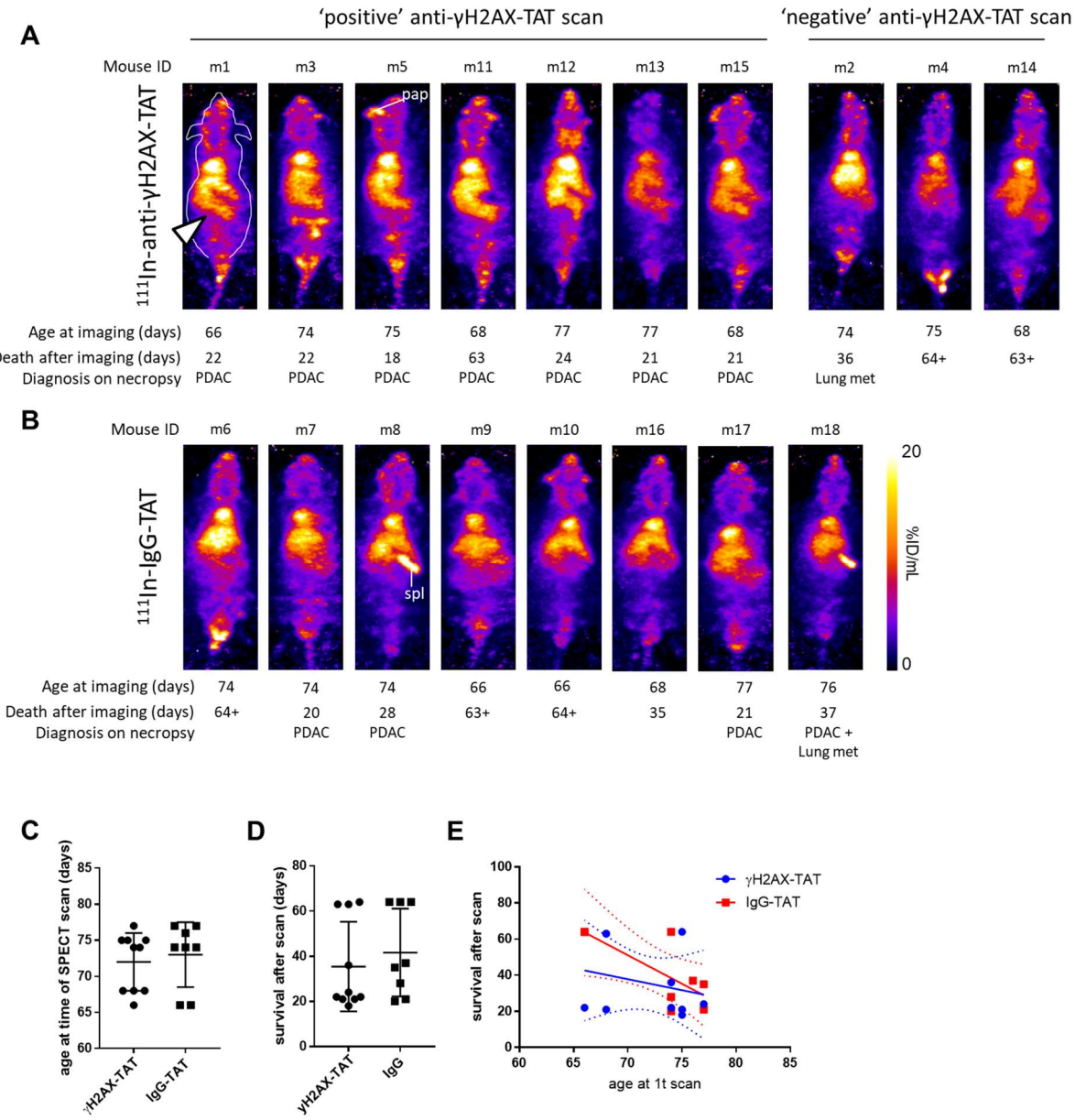

Supplemental Fig. 8 (A) KPC mice aged between 66-77 days were imaged by SPECT, 24 h after intravenous administration of ^{111}In-anti-γH2AX-TAT. Age at the time of imaging, the length of survival before clinical symptom endpoints were reached, and the diagnosis at necropsy are indicated for each mouse (Coronal MIPs are shown, an outline of a mouse is indicated for the first animal only). (B) Similar as (a), but using ^{111}In-IgG-TAT control compound. (C) The age at time of imaging was not significantly different between the different groups (ANOVA; P=0.99). (D) Survival after imaging was not significantly different in animals imaged with ^{111}In-anti-γH2AX-TAT or ^{111}In-IgG-TAT (P=0.51) (E) Survival time after imaging did not correlate with the age at the time of the scan, in this set of animals.